PAPER • **OPEN ACCESS**

Levitated cavity optomechanics in high vacuum

To cite this article: Uroš Deli *et al* 2020 *Quantum Sci. Technol.* **5** 025006

Quantum Science and Technology

OPEN ACCESS

RECEIVED
11 December 2019

REVISED
26 January 2020

ACCEPTED FOR PUBLICATION
24 February 2020

PUBLISHED
17 March 2020

PAPER

Levitated cavity optomechanics in high vacuum

Uroš Delić[1,4], David Grass[1,4,5], Manuel Reisenbauer[1], Tobias Damm[2,6], Martin Weitz[2], Nikolai Kiesel[1] and Markus Aspelmeyer[1,3]

[1] Vienna Center for Quantum Science and Technology (VCQ), Faculty of Physics, University of Vienna, Boltzmanngasse 5, A-1090, Vienna, Austria
[2] Institute for Applied Physics, University of Bonn, Wegelerstr. 8, D-53115, Bonn, Germany
[3] Institute for Quantum Optics and Quantum Information, Austrian Academy of Sciences, A-1090 Vienna, Austria
[4] UD and DG contributed equally to this work.
[5] Present address: Department of Chemistry, Duke University, Durham, NC 27708, United States of America.
[6] Present address: Bundesamt für Sicherheit in der Informationstechnik Godesberger Allee 185-189, D-53175, Bonn, Germany.

Keywords: optical levitation, nanoparticle, levitated cavity optomechanics, optomechanics, quantum cooperativity

Abstract

We report dispersive coupling of an optically trapped nanoparticle to the field of a Fabry–Perot cavity in high vacuum. We demonstrate nanometer-level control in positioning the particle with respect to the cavity field, which allows access to linear, quadratic, and tertiary optomechanical interactions in the resolved sideband regime. We determine all relevant coupling rates of the system, i.e. mechanical and optical losses as well as optomechanical interaction, and obtain a quantum cooperativity of $C_{\mathrm{Q}} = 0.01$. Based on the presented performance, the regime of strong cooperativity ($C_{\mathrm{Q}} > 1$) is clearly within reach by further decreasing the mode volume of the cavity.

1. Introduction

Cavity optomechanics enables optical quantum control of mechanical motion. Realized in a plethora of different platforms, it promises diverse applications ranging from quantum sensors to hybrid devices for quantum information processing, and it opens new ways to address fundamental questions in macroscopic quantum physics [1–4]. Current state of the art optomechanical systems include cryogenically cooled solid state devices coupled to superconducting microwave cavities or nanophotonic structures that, both, routinely operate in the quantum regime. Examples range from motional ground state laser cooling [5, 6] to the generation of quantum squeezed states [7–9], non-Gaussian states [10, 11] and entangled states [12–15] of micro-and nanomechanical motion.

Coupling the motion of a *levitated* object to an optical cavity provides new possibilities. At ultra-high vacuum, levitation enables excellent isolation of the mechanical motion from the environment, enhanced inertial sensitivity [16–20] as well as quantum optomechanics at room temperature. Furthermore, optical micromanipulation techniques can control the potential landscape, which allows access to anharmonic potentials, e.g. [21]. Switching the potential completely off allows free dynamics to be investigated with new approaches to force sensing and matter wave interferometry [20, 22, 23].

In its original form, levitated cavity optomechanics [24, 25] is realized by positioning an optically trapped particle inside an optical mode of a Fabry–Perot cavity. This configuration has first been suggested in [26–28] and builds on earlier work [29, 30]. The presence of the particle shifts the cavity resonance, which couples the particle motion dispersively to the cavity field, resembling the fundamental cavity optomechanical interaction. The first step in practically every quantum or sensing protocol is the preparation of a low entropy state, i.e. cooling the center of mass (COM) motion. In cavity optomechanics this is achieved by driving the cavity with a laser beam that is detuned by one mechanical frequency smaller than the cavity resonance frequency. Off-resonant (anti-Stokes) scattering will result in a cooling rate given by $\Gamma_{\mathrm{opt}} \approx 4g^2/\kappa$ (with linear optomechanical coupling strength g and the cavity linewidth κ), which competes with the heating rate Γ due to coupling to the thermal environment. Cavity cooling to the ground state (as well as coherent quantum control in the resolved

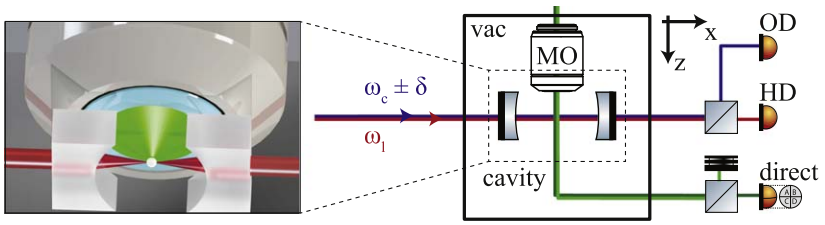

Figure 1. Experimental setup. A microscope objective (MO) and a trapping laser beam (dark green line, polarized along x-direction) form an optical tweezer holding a silica nanoparticle in vacuum. The particles center of mass motion is coupled to a high-Finesse Fabry–Perot cavity which is inside the same vacuum chamber (vac). The feedback laser beam (light green line, polarized along y-direction, perpendicular to the trapping laser) in combination with a three-dimensional position read-out (read-out) is used to cool the particle motion by parametric feedback. The frequency ω_l of a second laser beam (red line) is locked to the cavity resonance. The transmission of this laser is used for homodyne-detection (HD) to monitor the particle motion along the cavity axis (x). We derive a control mode (blue line) from the locked laser beam at frequency $\omega_c \pm \delta$ whose detuning can be arbitrarily chosen with respect to the cavity resonance frequency. For optomechanically induced transparency measurements the control mode is red-detuned with respect to the cavity resonance, phase modulated by a frequency δ and detected in transmission of the cavity (OD). To give an impression of the geometry for holding the particle with a high-NA objective in the center of the optical cavity, the inset shows a artistic view of the cavity and the microscope objective.

sideband regime) requires the ratio of these rates, the cooperativity C_Q, to exceed 1. This condition, $C_Q = 4g^2/\kappa\Gamma > 1$, is called the strong cooperativity regime.

Early experiments have achieved optical trapping of nanoparticles in a Fabry–Perot cavity with a cooperativity of $C_Q \approx 2 \times 10^{-6}$, limited by the environmental coupling at a gas pressure of 4 mbar [31]. At high vacuum levels, coupling to an optical cavity has been achieved for particles that were not continuously localized in the cavity field, i.e. they were either in transit through the cavity [32] or confined to a shallow Paul trap [33]. More recently, cooling of a levitated nanoparticle with a cavity to 10 mK in high vacuum has been demonstrated [34]. The largest dispersive shift up to now has been demonstrated for particles in transit through a microcavity [35] and in plasmonic trapping [36]. Photonic microcavities also enabled significantly enlarged coupling for trapped particles [37], but the cooperativity is still limited to $C_Q = 10^{-9}$ due to environmental pressure.

Here we demonstrate orders of magnitude improvement in cooperativity for a levitated nanoparticle that is positioned inside a high-finesse Fabry–Pérot cavity at high vacuum with an optical tweezer. We independently determine the optomechanical coupling rate g from optomechanically induced transparency (OMIT) measurements, the mechanical heating rate Γ via relaxation measurements [38] and the optical losses κ of the cavity. Based on these measurements we derive a quantum cooperativity $C_Q = 0.01$ for our present system. This value corresponds to an improvement by four orders of magnitude compared to a previous approach in which the particle was levitated by a cavity mode [27, 31] instead of a tweezer.

In this article, we first introduce the experimental setup, the technological developments necessary to combine a tweezer with a Fabry–Pérot cavity and the loading procedure in section 2. A detailed analysis of the coupling between the particle motion and the cavity, and the particle mass is presented in section 3. We proceed to characterize the mechanical heating rate Γ with relaxation measurements in section 4 and the optomechanical coupling rate g using OMIT measurements in section 5. These results allow us to estimate the quantum cooperativity and we lay out a route on how to reach the strong quantum cooperativity regime in section 6. The article is concluded in section 7.

2. Experimental setup

The experiment combines a free space Fabry–Pérot resonator with an optical tweezer as shown in figure 1. The optical tweezer is formed by a laser source at a wavelength of $\lambda = 1064$ nm and an optical power of $P = 0.17$ W (light green line, trapping laser). We focus the light using a microscope objective (MO, Olympus LMPL100x IR) of long working distance (WD = 3.4 mm) and high numerical aperture (NA = 0.8). The COM motion of a particle inside this Gaussian potential can be approximated by a three-dimensional harmonic oscillator with typical oscillation frequencies of $\Omega_x = 2\pi \times 163$ kHz and $\Omega_y = 2\pi \times 190$ kHz along the radial tweezer directions (x and y) and $\Omega_z = 2\pi \times 40$ kHz along the axial tweezer direction (z). The microscope objective is mounted on a triaxial nanopositioner such that the optical tweezer can be remotely positioned while a particle is in the trap. The particle COM motion is monitored in all three directions (standard detection, see [39]), using a collimation lens (NA = 0.16, not shown) to collect the forward scattered light. To cool the COM motion in all directions we apply parametric feedback cooling, i.e. we remove energy from the particle motion by introducing a velocity dependent spring constant (for a detailed description, see [39]). This requires a modulation of the tweezer power at twice the mechanical frequency of the nanoparticle motion. We implement this modulation

using a second laser beam (dark green line, feedback laser, derived from the trapping laser source), which is coupled into the same spatial mode as the trapping laser beam. To avoid interference, the feedback laser beam is orthogonally polarized and shifted in frequency by 82 MHz with respect to the trapping laser. The modulation signal is generated from the nanoparticle position read-out using three phase-locked loops. This ensures that the particle is stably levitated with the optical tweezer in high vacuum. With feedback cooling we obtain an effective COM temperature of $T_{\rm eff} \approx 100$ mK for each direction at the base pressure of our vacuum system of $p = 4.8 \times 10^{-7}$ mbar.

The optomechanical interface is realized with a high-finesse ($\mathcal{F} \approx 73000$), near-confocal Fabry–Pérot cavity. More specifically, we use mirrors with a radius of curvature of $R = 1$ cm separated by a length of $L = 1.07$ cm resulting in a free spectral range of $\Delta\omega = 2\pi \times 14.019$ GHz. The cavity is placed perpendicular with respect to the optical tweezer axis (along the x-axis, see figure 1). The substrate radius of the two cavity mirrors is originally $r_{\rm M} = 6.35$ mm. As the working distance of the microscope objective is shorter than the mirror radius WD $< r_{\rm M}$, a levitated particle inside the tweezer can not be positioned into the center of the cavity, where the optomechanical coupling is largest. Therefore we cut the mirrors into $d_{\rm M} = 4$ mm wide strips. The waist of the cavity mode is $w_0 = 41.1$ μm and its mode size on the mirror of $w(x = L/2) = 61$ μm is 65 times smaller than the width of the strip. The expected clipping losses are negligible compared with the design transmission of the cavity mirrors. With the reduced lateral extend of the cavity the microscope objective can be moved closer towards the cavity and a particle can be positioned on the cavity axis. The inset in figure 1 shows a schematic arrangement of the cut cavity mirrors, the microscope objective, the trapping laser (green) with a nanoparticle positioned in the cavity mode (red).

Two laser beams drive the Fabry–Pérot cavity (figure 1). The first beam (locking laser) is emitted from a second laser source ($\lambda = 1064$ nm, frequency $\omega_{\rm l}$, optical power $P \approx 50$ μW) which is stabilized to the cavity using a Pound–Drever–Hall locking scheme. The light of the locking laser transmitted through the cavity is used for homodyne detection (HD) of the particle COM motion along the cavity axis. A second laser beam with frequency $\omega_{\rm c} = \omega_{\rm l} + \Delta\omega + \Delta$ (control laser) is derived from the locking laser source: to this end, a fraction of the locking laser source is modulated with an electro-optical modulator (EOM) at frequency $\Delta\omega + \Delta$. One of the two created sidebands is selected with a filtering cavity with a bandwidth of $\kappa_{\rm FC} = 2\pi \times 100$ MHz. Thus, the control laser beam can be detuned by a variable frequency Δ with respect to the cavity mode that is one free spectral range $\Delta\omega$ away from the locking mode and can be power adjusted up to $P = 17$ mW to pump the control mode. This mode allows for optomechanical control such as cavity cooling. In addition, we can apply a phase modulation with frequency δ to the control mode $\omega_{\rm c}$ using the same EOM such that two sidebands are created at $\omega_{\rm c} \pm \delta$. These are used for OMIT measurements as described in section 5. The control mode and the locking mode are orthogonally polarized and separated with a polarizing beamsplitter in transmission of the optomechanical cavity for homodyne detection (HD) and OMIT detection (OD), respectively.

With the experimental setup in place, the loading of silica nanoparticles (radius $a = (71.5 \pm 2)$ nm, Microparticles GmbH) into the tweezer is based on a nebulizer approach [40]. A medical nebulizer (Omron MicroAIR U22) is filled with a solution of silica nanoparticles and isopropanol in a mass ratio of 1:10^4. The nebulizer creates small droplets of liquid at ambient pressure that are sucked into the pre-evacuated vacuum chamber. Here a nanoparticle is eventually trapped at a pressure of typically ~100 mbar. While the mass ratio between nanoparticles and solution allows for reproducible trapping in the optical tweezer, it turned out detrimental for the cavity mirrors. We observed a reduction in finesse from $\mathcal{F} = 200\,000$ to $\mathcal{F} = 40\,000$ after a single loading attempt. To avoid contamination of the mirrors we designed our experiment in a modular fashion that allows removal of the optical cavity [41]: the two cavity mirrors are glued into an aluminium mount which can be manually removed (inserted) from (into) the vacuum chamber via a CF quick access door. The cavity is not present during the loading procedure and only put back in place when a particle is levitated in the tweezer.

3. Characterization of optomechanical coupling and particle mass

The setup presented above allows to change the position of a nanoparticle precisely with respect to the optical cavity. In the following we study the dependence of the optomechanical coupling on the particle position. It is convenient to separate the particle motion along the cavity axis $x = x_0 + \hat{x}$ into its average position x_0, the position of the potential minimum of the tweezer and its oscillatory motion $\hat{x}$ around x_0 (the same can be done for the remaining directions). The cavity frequency shift per photon as function of the particle position is given by [27, 42]

$$U(x, y, z) = \frac{\omega_l \alpha}{2\varepsilon_0 V_c} \frac{w_0^2}{w^2(x_0)} e^{-\frac{y_0^2+z_0^2}{w^2(x_0)}} \sin^2(kx) = U_0 \sin^2(kx) \tag{1}$$

with the particle polarizability $\alpha = 4\pi\varepsilon_0 a^3(\varepsilon - 1)/(\varepsilon + 2)$, the vacuum permittivity ε_0, the dielectric constant of the particle ε, the cavity mode volume $V_c = \pi w_0^2 L/4$, the cavity waist function $w(x) = w_0\sqrt{1 + (x/x_R)^2}$ and the Rayleigh length of the cavity mode x_R. Note that $U_0 = U_0(x_0, y_0, z_0)$ is a function of the particle's average position. The change of resonance frequency of the cavity, see equation (1), gives rise to the optomechanical coupling and is described by the interaction Hamiltonian

$$\begin{aligned} H_{\text{int}} &= -\hbar\sqrt{n_l}\,U_0 \sin^2\left[k(x_0 + \hat{x})\right](\hat{a}_l^\dagger + \hat{a}_l) \\ &\approx -\hbar\sqrt{n_l}\left[g_0\frac{\hat{x}}{x_{\text{zpf}}} + g_q\frac{\hat{x}^2}{x_{\text{zpf}}^2} - g_c\frac{\hat{x}^3}{x_{\text{zpf}}^3}\right](\hat{a}_l^\dagger + \hat{a}_l) \end{aligned} \tag{2}$$

with the intracavity cavity photon number n_l of the locking mode and the zero-point fluctuation of the particle motion x_{zpf}. The approximation results from a Taylor expansion of the sinusoidal function around x_0 to third order and dropping the constant term. We also introduced the linear single photon coupling $g_0 = x_{\text{zpf}}\,kU_0\sin(2kx_0)$, the quadratic coupling $g_q = x_{\text{zpf}}^2 k^2 U_0\cos(2kx_0)$ and the cubic coupling $g_c = \frac{2}{3}x_{\text{zpf}}^3 k^3 U_0\sin(2kx_0)$.

The three terms in the interaction Hamiltonian lead to a modulation of the cavity susceptibility at the respective harmonics of the mechanical frequency. Experimentally, this is reflected in a phase modulation of the locking beam transmitted through the optical cavity and can be detected with homodyne detection. The amplitudes of the detected signals at their corresponding harmonics allow direct inference of linear, quadratic and cubic coupling. A more detailed description can be found in appendix A. This also serves as alignment signal to position the optical tweezer with respect to the cavity mode. For example, linear coupling between the particle motion and the cavity can be achieved in the following way: When the particle is in proximity of the cavity field, the tweezer position is systematically changed until the first harmonic (linear coupling) of the COM motion is maximized and the second harmonic (quadratic coupling) is simultaneously minimized.

In a first measurement we move the particle along the y-axis (z-axis) through the cavity mode, record a homodyne spectrum at each position, and extract the peak height $\propto U_0(x_0, y_0, z_0)$ at the mechanical frequency Ω_x. The frequency shift introduced by the particle resembles the Gaussian envelope of the cavity mode, see equation (1). Our measured value for the waist along the y-direction (z-direction) is $w_y = (42.3 \pm 1.2)\ \mu$m ($w_z = (41.8 \pm 1.2)\ \mu$m), which agrees well with the waist $w_0 = 41.1\ \mu$m we expect from calculations based on radius of curvature and cavity length. In a second measurement we position the particle on the cavity axis ($y_0 = z_0 = 0$), scan the levitated particle along the cavity axis x in steps of 8 nm and record a homodyne spectrum at each position. We use the spectrum, as described in appendix A, to map out the linear (blue), quadratic (red) and cubic (green) coupling strengths as a function of position (figure 2(b)).

The modulation of the locking beam via the particle can also be used to measure the mass of the levitated nanoparticle. The amplitude of the nanoparticle motion enters with different powers for linear, quadratic and cubic coupling. A relative comparison between the amplitude of the first harmonic motion (Ω_x) at the position of maximal linear single photon coupling ($\sin(2kx_0) = 1$) with the amplitude of the second harmonic motion ($2\Omega_x$) at the position of maximal quadratic single photon coupling ($\cos(2kx_0) = 1$) and using the fact, that the particle is in equilibrium with its thermal environment allows for a determination of the particle's mass: $m = (2.86 \pm 0.04)$ fg, see appendix B. The sensitivity of this purely optical mass measurement is comparable to recently published electro-optical methods [43, 44]. Using the manufacturer specification for the density of silica $\rho = 1850\ \text{kg m}^{-3}$ and assuming a spherical shape, we calculate a nanoparticle radius of $a = (71.8 \pm 0.9)$ nm, in good agreement with the value of $a = (71.5 \pm 2)$ nm specified by the manufacturer. With the independently characterized values for particle mass, particle radius, mechanical frequency, cavity waist and cavity length we infer a single photon coupling rate of $g_0 = 2\pi \times 0.3$ Hz.

In addition, the locking field exerts a weak gradient force onto the nanoparticle, modifying its optical potential. When the particle is moved along the cavity axis, this effect is observed in a position dependent modulation of the mechanical frequency $\Omega_x' = \Omega_x + 2g_q n_l\cos(2kx_0)$ as displayed in figure 2(a). The yellow dots represent data points, the solid line is a fit with the intracavity photon number n_l as the only free fit parameter and the red-black shaded background indicates the intensity of the cavity field. The intensity of the cavity field is based on measurement of the optical power leaking out of the cavity, the transmission of the output coupler and the measured waist of the cavity mode. At a high intensity region the additional confinement of the cavity field increases the mechanical frequency and vice versa at the cavity field node. Both measurement routines consistently determine the tweezer position with respect to the cavity field and are used to control the coupling between the particle COM motion and cavity field accordingly.

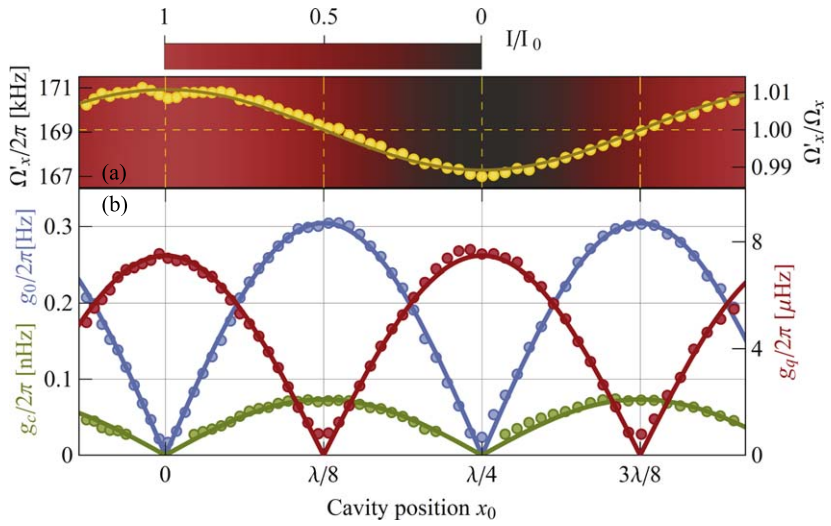

Figure 2. Position dependent frequency and optomechanical coupling. (a) The mechanical frequency Ω_x follows the intensity profile (background colour) as we move the nanoparticle along the cavity standing wave. The cavity adds a positive (negative) spring constant at the intensity maximum $x_0 = 0$ (minimum $x_0 = \lambda/4$). The corresponding frequency variation is proportional to intracavity photon number of the locking mode. (b) Different orders of dispersive optomechanical coupling: The linear single photon coupling g_0 (blue) is maximal at the intensity slope ($x_0 = \lambda/8$ and $x_0 = 3\lambda/8$) as well as the cubic coupling g_c (green). Quadratic coupling g_q (red) is optimal at the extrema of the intensity distribution.

4. Mechanical heating rate Γ

The coherent optomechanical interaction competes with noise acting on the nanoparticles COM motion. The noise originates from two contributions: on one hand collisions with surrounding gas molecules result in a heating rate $\Gamma_p = \bar{n}_{th}\gamma_p$, with γ_p the pressure dependent mechanical linewidth [45] and $\bar{n}_{th} = k_B T_0/(\hbar\Omega_x)$ the thermal occupation of the bath. On the other hand, the nanoparticle scatters photons off the optical trap, effectively creating a white and Gaussian but anisotropic force noise. The resulting recoil heating rate along the cavity axis is $\Gamma_{rc} = I\sigma_{sc}k/(10mc\,\Omega_x)$, with $k = 2\pi/\lambda$, I the intensity of the light field at the particle position, σ_{sc} the scattering cross section of the particle and c speed of light [38].

The recoil heating is dominated by the trapping field of the tweezer but has, in principle, also a contribution from the control and the locking field of the cavity. In our current regime of operation, however, these contributions can be neglected as the intensity of the trapping laser $I_{tw} = 2.1 \times 10^{11}\,\mathrm{W\,m^{-2}}$ is much higher than the intensity of the locking mode $I_l = 1.2 \times 10^{8}\,\mathrm{W\,m^{-2}}$ and the intensity of the control mode $I_c = 2 \times 10^{9}\,\mathrm{W\,m^{-2}}$ at maximum coupling: $I_{tw} \gg I_c \gg I_l$. In addition, at the base pressure of our vacuum system ($p = 4.8 \times 10^{-7}$ mbar) the pressure dependent heating rate $\Gamma = 2\pi \times 28$ kHz still dominates over the expected recoil heating rate of $\Gamma_{rc} = 2\pi \times 4.4$ kHz.

First, we measure the pressure dependent heating rate in the optical tweezer without the cavity fields present. We employ two complementary measurement protocols: relaxation measurements analogous to [38] in a pressure regime where feedback cooling is efficient ($p < 1$ mbar) and for higher pressures ($p > 1$ mbar) we determine the linewidth of the mechanical oscillator from the noise power spectrum. In a relaxation measurement all three directions of motion are prepared in a low energy state $E_0 \ll E_\infty$ using parametric feedback cooling. After switching off the cooling, the mean particle energy evolves according to:

$$E(t) = E_\infty + (E_0 + E_\infty)\mathrm{e}^{-\gamma t} \approx E_0 + \Gamma t, \tag{3}$$

with $\Gamma = \gamma E_\infty$, $\gamma = \gamma_p + \gamma_{rc}$ the combined mechanical linewidth, γ_{rc} the recoil linewidth and E_∞ the equilibrium energy [38]. Experimentally, we perform approximately 5000 repetitions of a relaxation measurement at a set of pressures ranging between ≈100 mbar and the base pressure of the vacuum system.

The energy is computed as an ensemble variance $E(t) \propto \langle x^2\rangle(t)$ of all 5000 relaxation trajectories. The resulting energy relaxation curves are shown for two cases in figure 3. In part (b) the complete relaxation is monitored, as the particle can be reliably levitated without feedback control until a pressure of $p = 0.56$ mbar. Below this pressure, the particle might escape the trap due to a still unknown heating mechanism and we therefore switch feedback cooling off for a fraction of the relaxation time (inverse mechanical linewidth $1/\gamma$) and measure only the linear part of the relaxation trajectory. The solid black line is a fit of the energy data (red shaded area) to equation (3) with γ, E_0 and E_∞ as free fit parameters. The yellow area indicates the time while feedback cooling is enabled. We infer the mechanical heating rates $\Gamma = \Gamma_p + \Gamma_{rc}$ either directly from the linear fit or,

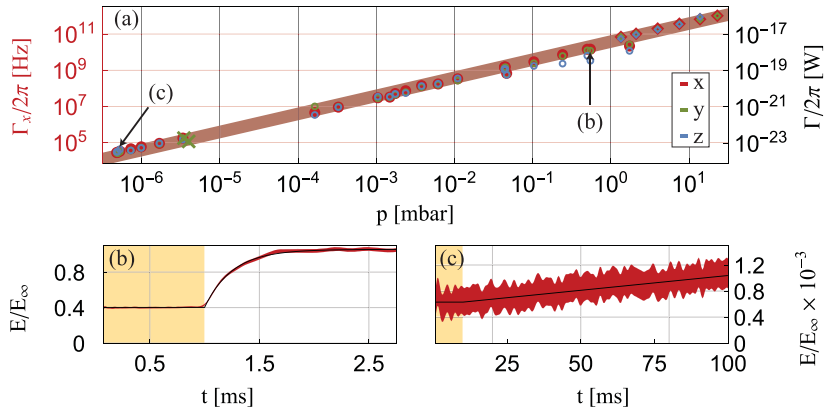

Figure 3. Pressure dependent mechanical heating rate. (a) Mechanical heating rate $\Gamma_x/2\pi$ of a levitated particles center-of-mass motion along the cavity axis (x) as a function of pressure (red symbols). We measure the mechanical losses either via energy relaxation (circles and dots) at low pressures or via a spectral method (diamonds) at higher pressures. The phonon heating rate $\Gamma_x/2\pi$ ([phonon/s], left y-axis in red) solely applies for the motion along the cavity as it depends on direction. The energy heating rate $\Gamma/2\pi$ ([W], right y-axis in black) is expected equal in all spatial directions and applies to all data points. The red shaded area is a theory curve whose width accounts for the uncertainties in system parameters (pressure, particle radius, mechanical frequency, equilibrium temperature) during the measurement. The two crosses mark heating rates with the cavity field on, showing that the cavity field has a negligible influence on heating. (b) and (c) energy relaxation measurement: the particle is prepared in a low energy state with feedback cooling (yellow shaded area). After switching feedback cooling off, the particle relaxes towards thermal equilibrium. At a pressure of $p \approx 0.56$ mbar (b), the full relaxation to thermal equilibrium is observed, while for lower pressures, i.e. $p = 4.8 \times 10^{-7}$ mbar (c) only the linear part of the relaxation is measured.

when full relaxation is possible, from the product $\Gamma = \gamma E_\infty$. For pressures above 1 mbar we fit the mechanical linewidth γ of a mechanical noise power spectrum and compute the heating rate via $\Gamma = \gamma E_\infty$. Figure 3(a) summarizes the mechanical loss measurements as a function of pressure. The COM motion along the cavity axis (x) is plotted in red (quantified by the left y-scale: $\Gamma_x/2\pi$ [phonon/s]). The red shaded area is the theoretical prediction including all measurement uncertainties (pressure, particle radius, mechanical frequency, equilibrium temperature). The mechanical heating rate along the y direction (z direction) is plotted in green (blue) color. Together with the x direction they share the right y-scale: $\Gamma/2\pi$ in units of Watts. The circles and dots represent relaxation measurements and the diamonds spectral measurements. As expected, in the air collision dominated regime $\Gamma_p \gg \Gamma_{rc}$, the regime we are currently operating at, the mechanical losses are isotropic.

Second, to test the assumption that the cavity field has a negligible impact on the heating rate, we perform two relaxation measurements along the y-axis while the two cavity fields are present (green crosses). As expected, this causes no significant increase in heating rate compared to the case without cavity fields. At the base pressure of the vacuum system we measure the minimal mechanical heating rate along the cavity axis of $\Gamma = 2\pi \times 28$ kHz.

5. Optomechanically induced transparency

To characterize the cooperativity C_Q of our system we need to measure the coupling g between optics and mechanics. We choose optomechanically induced transparency (OMIT, [46, 47]), a phenomenon in close analogy to electronically induced transparency in atom quantum optics [48]. OMIT results from a modification of the cavity response in the presence of optomechanical interaction. More specifically, when the cavity is driven by a control laser (red-detuned from the cavity resonance by the mechanical frequency), near resonant light from a probe laser cannot enter the cavity. This effect is best understood in a scattering picture. The optomechanical interaction between particle and control mode scatters photons into the Stokes (far off-resonant) and anti-Stokes (resonant) sidebands of the control laser. Destructive interference between the anti-Stokes photons and the probe laser photons in the cavity causes a reduced transmission of probe laser photons. The reduction in transmission of the probe laser is determined by the number of scattered photons, which only depends on the optomechanical coupling and not on the mechanical linewidth.

Before each measurement the single photon coupling g_0 between the particle and the control mode is maximized. As the particle is close to the longitudinal center of the optical cavity $x_0 \approx 0$, we can achieve this by maximizing the linear coupling g_0 between the COM motion and the locking laser (see section 2). Then, we switch on the control laser whose power determines the intracavity photon number n_c and therefore the optomechanical coupling $g = \sqrt{n_c} g_0$. The probe laser is derived from the control laser by sideband modulation.

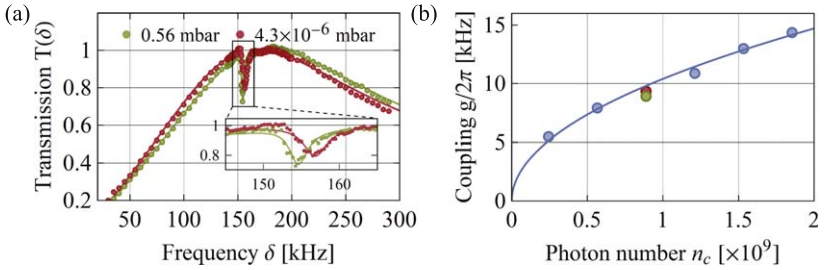

Figure 4. Optomechanically induced transparency (OMIT) and optomechanical coupling rate g. (a) OMIT measurements: the cavity transmission of the probe beam is measured (OD) as a function of the probe modulation frequency δ at a pressure of $p = 0.56$ mbar (green) and $p = 4.3 \times 10^{-6}$ mbar (red). The envelope of the response is defined by the cavity linewidth κ and the red-detuning of the control mode Δ. The narrow dip is present at $\delta = \Omega_x \approx 2\pi \times 155$ kHz due to destructive interference between nanoparticle motion and probe mode. It allows us to infer the optomechanical coupling rate g. Inset: Zoom-in of the transparency window. The two curves differ due to a drift in detuning, which has no effect on the coupling rate. (b) Optomechanical coupling rate $g = g_0\sqrt{n_c}$ as a function of intracavity photon number n_c. Blue and green data points were measured at a pressure of $p = 0.56$ mbar and the red data point at $p = 4.3 \times 10^{-6}$ mbar, which indicates that the coupling is pressure independent. The solid line is a theoretical prediction based on the single photon coupling g_0 and the intracavity photon number n_c. Note that the color coding in part (a) matches the two data points in part (b).

More specifically, we phase modulate the control laser at a frequency δ creating two sidebands at $\omega_c \pm \delta$. One of them is far off-resonant with respect to the cavity and strongly suppressed (because ω_c is chosen to be red-detuned) while the other one is used to probe the transmission near the cavity resonance.

Figure 4(a) shows the normalized cavity transmission of the probe beam (detected with OD) as a function of the modulation frequency δ for two different pressures in the vacuum chamber (green: 0.56 mbar, red: 4.3×10^{-6} mbar), i.e. two dissipation rates. The transparency window of the probe laser is clearly visible at the cavity resonance, in our case as a narrow window of reduced transmission. For a quantitative analysis the Stokes sideband, both modulation sidebands and the cavity linewidth have to be taken into account. Therefore the coupling g is derived from a fit to the probe transmission with three free parameters: the mechanical linewidth γ, the red-detuning Δ and the mechanical frequency Ω_{m} (a more detailed description including the functional form for fitting can be found in [49]).

We use this method to study the dependence $g = \sqrt{n_c}g_0$ of the optomechanical coupling rate on the intracavity photon number, i.e. the control laser power. The results are plotted in figure 4(b) as data points and the solid line is a theoretical prediction based on the independently measured value for the single photon coupling g_0 (section 3) and the measured intracavity photon number n_c. The expected square root dependence is clearly observable in the data and the good agreement between theory curve and data confirms our value for g_0. All measurements were performed at a pressure of $p = 0.56$ mbar except for the red data point ($p = 4.3 \times 10^{-6}$ mbar). The measurement at lower pressure fits very well into the data at higher pressures and indicates that the optomechanical coupling is, as expected, pressure independent. The two data points highlighted in green and red correspond to the measurements in shown in figure 4(a).

6. Cooperativity

With the measured value for the optomechanical coupling $g = 2\pi \times 9.6$ kHz, the mechanical heating $\Gamma = 2\pi \times 175$ kHz at a pressure of $p = 4.3 \times 10^{-6}$ mbar and the optical losses $\kappa = 2\pi \times 193$ kHz we find a value for the quantum cooperativity of our current experimental setup of $C_{\mathrm{Q}} = 0.01$. We have a clear route to further improve the system to reach the desired strong quantum cooperativity regime $C_{\mathrm{Q}} > 1$.

An obvious improvement is to operate at lower pressures to reduce the mechanical heating rate Γ. The optomechanical coupling of $g = 2\pi \times 9.6$ kHz was measured at a pressure of $p = 4.3 \times 10^{-6}$ mbar and not at the base pressure of the current vacuum system $p = 4.8 \times 10^{-7}$ mbar with a mechanical heating of $\Gamma = 2\pi \times 28$ kHz. In combination with the maximal measured coupling rate $g = 2\pi \times 14.4$ kHz, see figure 4, a cooperativity of $C_{\mathrm{Q}} = 0.15$ is expected. The mechanical heating can be further minimized until the recoil limit is reached, i.e. $\Gamma_{\mathrm{p}} = \Gamma_{\mathrm{rc}}$. For our experiment, this is expected to happen at a pressure of $p \approx 10^{-7}$ mbar and would result in a quantum cooperativity of $C_{\mathrm{Q}} = 0.48$.

The quantum cooperativity $C_{\mathrm{Q}} = 4n_c g_0^2/(\kappa\Gamma)$ becomes larger for more intracavity photons n_c, i.e. by increasing the control beam power. This was already demonstrated for the OMIT measurements, see figure 4(a), but increasing the intra-cavity power alters the optical potential for the nanoparticle. If the control mode power becomes too strong, the gradient force will pull the particle towards the next anti-node away from the linear slope and reduce the coupling by self-trapping. This effect was already measured for weak intracavity powers in a

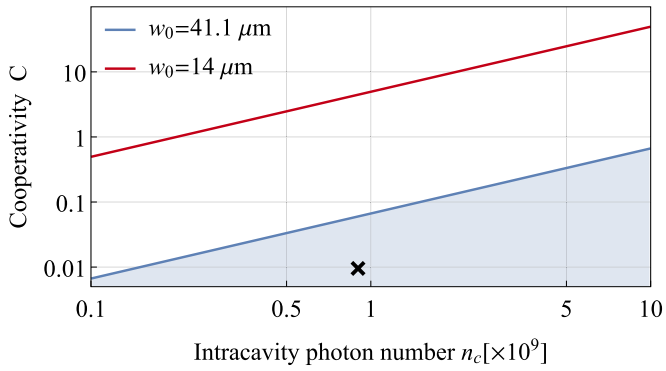

Figure 5. Projected cooperativity C_Q as a function of intracavity photon number n_c: the blue shaded area represents the values of C_Q accessible with our current experimental setup and the black cross represents the experimentally measured value of $C_Q = 0.01$. Even if operated at the base pressure of our vacuum system (solid blue line) the strong cooperativity regime cannot be reached. If we modify the Fabry–Pérot resonator to a smaller optical mode ($w_0 = 14$ μm), with our current setup we expect to be able to access the strong cooperativity regime of $C_Q > 1$.

shift of the mechanical oscillation frequency, see figure 2(a). Note that the effect of self-trapping can be partially compensated using the restoring force of the optical tweezer, in other words by using the optical tweezer to pull the particle back to the point of optimal coupling.

Even a combination of both, more intracavity photons and operation in the recoil limit will not suffice to reach the strong quantum cooperativity regime with our current system. This is illustrated by the blue curve in figure 5 as a function of intracavity photon number and for operation at the base pressure.

A way out to further increase the cooperativity is an improved cavity design. The cooperativity scales like $C_Q \propto V_{cav}^{-2}$ with the cavity mode volume $V_{cav} = Lw_{cav}^2/4$ (see [49]). A reduction of the current cavity waist from $w_{cav} = 41$ μm to a value of $w_0 = 14$ μm, would allow us to reach the strong quantum cooperativity regime, even with moderate intracavity powers as shown by the red curve in figure 5.The cavity waist can be reduced by either using a concentric cavity geometry like for example in [50] or a geometrically asymmetric cavity [51]. A geometrically asymmetric cavity consists of one normal, macroscopic mirror and one micro-mirror with a radius of curvature on the order of 100 μm. Both designs would not change the length of the cavity, support a waist of $w_0 = 14$ μm, and could be easily incorporated into our current experimental setup. Note that there are recent results on coherent scattering [52, 53] as an alternative approach to dispersive coupling between particle motion and cavity field. A combination of the coherent scattering protocol [52] with the high vacuum operation of this experimental platform offers a second path to access the regime of strong quantum cooperativity.

7. Conclusion

We have demonstrated dispersive coupling of a levitated nanoparticle in high vacuum ($p = 4.3 \times 10^{-6}$ mbar) to a high-finesse optical cavity. Excellent control over the nanoparticle position with respect to the cavity allowed us to observe linear, quadratic, and cubic optomechanical coupling. We have determined the heating rates of the nanoparticles' center-of-mass motion and employed optomechanically induced transparency to measure its coupling to the cavity field. This constitutes a complete toolbox to determine the optomechanical cooperativity. With the measured value for the optomechanical coupling of $g = 2\pi \times 9.6$ kHz, the mechanical heating rate $\Gamma = 2\pi \times 175$ kHz at a pressure of $p = 4.3 \times 10^{-6}$ mbar, and the optical losses $\kappa = 2\pi \times 193$ kHz we find a value for the quantum cooperativity of $C_Q = 0.01$. This is a major step towards the regime of strong quantum cooperativity ($C_Q > 1$) in room temperature optomechanical systems. We believe our experimental toolbox provides an important contribution for quantum protocols that have been envisioned for levitated nanoparticles throughout the last decade, like quantum state preparation and matter-wave interferometry for tests of macroscopic quantum physics.

Acknowledgments

This project was supported by the European Research Council (ERC CoG QLev4G), by the ERA-NET programme QuantERA, QuaSeRT (Project No. 11299191; via the EC, the Austrian ministries BMDW and BMBWF and research promotion agency FFG), by the Austrian Science Fund (FWF): START program (Project

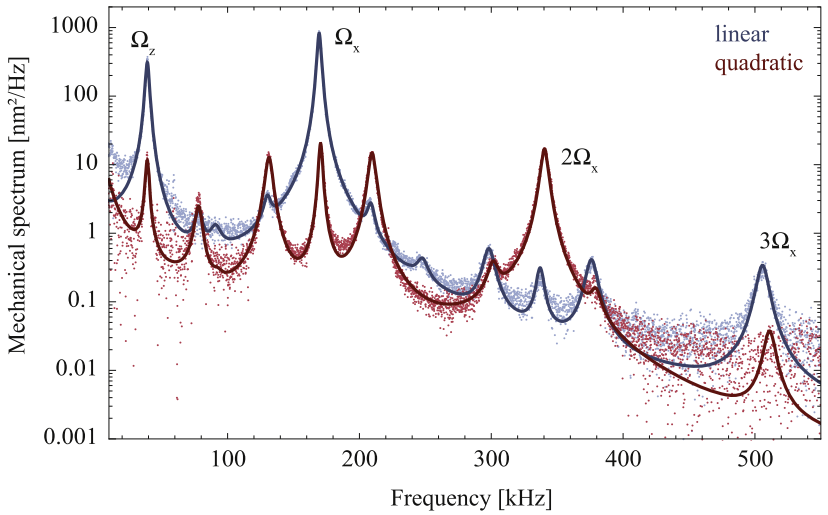

Figure A1. Two mechanical spectra of a levitated nanoparticle measured at a position of maximum linear coupling (blue) and maximum quadratic coupling (red) with the cavity homodyne read-out. The first peak Ω_z is a remnant of the axial particle motion (along z-axis) and the following three main peaks are the linear, quadratic and cubic particle x-motion. Note that, due to the nonlinearity of cavity read-out and the absence of cooling in this measurement, the x-motion is modulation by the z-motion which is manifested in sidebands of the harmonics of the x-motion.

Y 952-N36) and the doctoral school CoQuS (Project W1210), and the research platform TURIS at the University of Vienna. We thank Lorenzo Magrini for valuable discussions.

Appendix A. Homodyne spectrum and optomechanical couplings

The recorded homodyne spectrum of the cavity phase quadrature allows us to read out the harmonics of the nanoparticle motion, with its functional dependence given by [49]

$$S_{YY}(\omega) \propto \left(\frac{\bar{g}_0 \sin(2kx_0)}{x_{\mathrm{zpf}}}\right)^2 S_{xx}(\omega) + \left(\frac{\bar{g}_\mathrm{q} \cos(2kx_0)}{x_{\mathrm{zpf}}^2}\right)^2 S_{x^2x^2}(\omega) + \left(\frac{\bar{g}_\mathrm{c} \sin(2kx_0)}{x_{\mathrm{zpf}}^3}\right)^2 S_{x^3x^3}(\omega) + \cdots, \tag{A.1}$$

where the linear, quadratic and cubic optomechanical coupling rates are

$$\begin{aligned} g_0(x_0) &= x_{\mathrm{zpf}} k U_0 \sin 2kx_0 = \bar{g}_0 \sin 2kx_0 \\ g_\mathrm{q}(x_0) &= (x_{\mathrm{zpf}} k)^2 U_0 \cos 2kx_0 = \bar{g}_\mathrm{q} \cos 2kx_0 \\ g_\mathrm{c}(x_0) &= \frac{2}{3}(x_{\mathrm{zpf}} k)^3 U_0 \cos 2kx_0 = \bar{g}_\mathrm{c} \cos 2kx_0, \end{aligned} \tag{A.2}$$

and x_0 is the average particle position. We move the nanoparticle along the cavity standing wave in steps of 8 nm (given by the nanopositioner minimal step size) and record a homodyne spectrum at each position. By controlling x_0 along the standing wave, the cavity interaction can be tuned from an optimized readout of the linear x-motion (figure A1, blue curve) to a readout which is most sensitive to the quadratic x^2-motion (figure A1, red curve). We fit equation (A.1) to the position of maximal linear single photon coupling ($\sin(2kx_0) = 1$) and use the independently inferred value for g_0, x_{zpf} and the linear mechanical spectrum S_{xx} (see equation (B.2)) to find the calibration constant between the left and right side of equation (A.1). Note that, for simplicity, we do not explicitly treat the sidebands imprinted on the x-motion, see figure A1, which are caused by a modulation of the z-motion due to a nonlinearity in the cavity read-out and the absence of cooling in this measurement. This procedure works well in the underdamped regime ($\Omega_x \gg \gamma_m$), as this condition implies that $S_{xx}(\omega)$, $S_{x^2x^2}$ and $S_{x^3x^3}(\omega)$ have vanishing overlap. From here on, the linear single photon coupling $g_0(x_0)$, the quadratic single photon coupling $g_\mathrm{q}(x_0)$ and the cubic single photon coupling $g_\mathrm{c}(x_0)$ are a direct result from fitting of the homodyne spectrum, as shown in figure 2 in the main text.

Appendix B. Particle mass measurement

In the underdamped regime ($\Omega_x \gg \gamma$), the spectrum of the second harmonic motion $S_{x^2x^2}$ is given by [54]:

$$S_{x^2x^2}(\omega) = \frac{64\gamma_m\Omega_x^2}{(\omega^2+\gamma_m^2)((\omega^2-(2\Omega_x)^2)^2+4\omega^2\gamma_m^2)}\left(\frac{k_B T}{m\Omega_x^2}\right)^2. \tag{B.1}$$

The linear mechanical spectrum is given by [3]:

$$S_{xx}(\omega) = \frac{k_B T}{m\Omega_x^2}\frac{2\gamma_m\Omega_x^2}{(\omega^2-\Omega_x^2)^2+\omega^2\gamma_m^2}. \tag{B.2}$$

At the position of maximal linear coupling ($\sin(2kx_0) = 1$), fitting of equation (A.1) allows us to define a coefficient for the first harmonic of the particle motion $a_x \propto (\bar{g}_0/x_{zpf})^2 S_{xx}(\Omega_x)$. At the position of maximal quadratic coupling ($\cos(2kx_0) = 1$), the same can be done for the second harmonic motion $a_{x^2} \propto (\bar{g}_q/x_{zpf}^2)^2 S_{x^2x^2}(2\Omega_x)$. The ratio of both coefficients

$$\frac{a_{x^2}}{a_x} = \frac{\bar{g}_q{}^2 S_{x^2x^2}(2\Omega_x)}{\bar{g}_0{}^2 x_{zpf}^2 S_{xx}(\Omega_x)} = k^2\frac{k_B T}{4m\Omega_x^2} \tag{B.3}$$

is solely a function of the wavenumber $k = 2\pi/\lambda$, the Boltzmann constant k_B, the environmental temperature T, the mechanical frequency Ω_x and the particle mass m. Thus, if we assume that the bath temperature is $T \sim 293$ K (which is reasonable at pressures of $p > 1$ mbar, at which this measurement was conducted), all parameters are known, and hence, we can extract the nanoparticle mass as

$$m = \frac{k^2 k_B T}{4\Omega_x^2}\frac{a_x}{a_{x^2}}. \tag{B.4}$$

Note that this is a relative measurement of two spectral peaks, i.e. it is not necessary to have a calibrated spectrum. This also means that the mass measurement can be performed without knowledge of g_0. We obtain a nanoparticle mass of $m = (2.86 \pm 0.04)$ fg using equation (B.4), extremely close to the calculated mass of $m = 2.83$ fg based on a density of $\rho = 1850\,\mathrm{kg\,m^{-3}}$ and a radius of $r = 71.5$ nm, specified by the manufacturer. From the specified density $\rho = 1850\,\mathrm{kg\,m^{-3}}$ we estimate the nanoparticle radius to be $r = (71.8 \pm 0.9)$ nm, which fits extremely well to the nominal radius $r = (71.5 \pm 2)$ nm. We can also use the ratio between the quadratic and cubic coupling a_{x^3} (defined analogous to a_x and a_{x^2})

$$m = \left(\frac{2}{3}\right)^2\frac{k^2 k_B T}{4\Omega_x^2}\frac{a_x^2}{a_{x^3}} \tag{B.5}$$

to infer the radius, albeit with a larger error: $r = (71.5 \pm 1.5)$ nm.

ORCID iDs

David Grass https://orcid.org/0000-0003-1781-0969
Nikolai Kiesel https://orcid.org/0000-0002-0352-8279

References

[1] Kippenberg T J and Vahala K J 2008 Cavity optomechanics: back-action at the mesoscale *Science* **321** 1172–6
[2] Aspelmeyer M, Meystre P and Schwab K 2012 Quantum optomechanics *Phys. Today* **65** 29–35
[3] Aspelmeyer M, Kippenberg T J and Marquardt F 2014 Cavity optomechanics *Rev. Mod. Phys.* **86** 1391–452
[4] Bowen W P and Milburn G J 2015 *Quantum Optomechanics* 1st edn (Boca Raton, FL: CRC Press)
[5] Teufel J D, Donner T, Li D, Harlow J W, Allman M S, Cicak K, Sirois A J, Whittaker J D, Lehnert K W and Simmonds R W 2011 Sideband cooling of micromechanical motion to the quantum ground state *Nature* **475** 359–63
[6] Chan J, Alegre T, Safavi-Naeini A H, Hill J T, Krause A, Gröblacher S, Aspelmeyer M and Painter O 2011 Laser cooling of a nanomechanical oscillator into its quantum ground state *Nature* **478** 89–92
[7] Wollman E E, Lei C U, Weinstein A J, Suh J, Kronwald A, Marquardt F, Clerk A A and Schwab K C 2015 Quantum squeezing of motion in a mechanical resonator *Science* **349** 952–5
[8] Pirkkalainen J-M, Damskägg E, Brandt M, Massel F and Sillanpää M A 2015 Squeezing of quantum noise of motion in a micromechanical resonator *Phys. Rev. Lett.* **115** 243601
[9] Lecocq F, Clark J B, Simmonds R W, Aumentado J and Teufel J D 2015 Quantum nondemolition measurement of a nonclassical state of a massive object *Phys. Rev.* X **5** 041037
[10] O'Connell A D *et al* 2010 Quantum ground state and single-phonon control of a mechanical resonator *Nature* **464** 697–703
[11] Hong S, Riedinger R, Marinković I, Wallucks A, Hofer S G, Norte R A, Aspelmeyer M and Gröblacher S 2017 Hanbury Brown and Twiss interferometry of single phonons from an optomechanical resonator *Science* **358** 203–6
[12] Palomaki T A, Teufel J D, Simmonds R W and Lehnert K W 2013 Entangling mechanical motion with microwave fields *Science* **342** 710–3

[13] Riedinger R, Wallucks A, Marinković I, Löschnauer C, Aspelmeyer M, Hong S and Gröblacher S 2018 Remote quantum entanglement between two micromechanical oscillators *Nature* **556** 473–7
[14] Marinković I, Wallucks A, Riedinger R, Hong S, Aspelmeyer M and Gröblacher S 2018 Optomechanical bell test *Phys. Rev. Lett.* **121** 220404
[15] Ockeloen-Korppi C F, Damskägg E, Pirkkalainen J-M, Asjad M, Clerk A A, Massel F, Woolley M J and Sillanpää M A 2018 Stabilized entanglement of massive mechanical oscillators *Nature* **556** 478–82
[16] Gieseler J, Novotny L and Quidant R 2013 Thermal nonlinearities in a nanomechanical oscillator *Nat. Phys.* **9** 806–10
[17] Ranjit G, Atherton D P, Stutz J H, Cunningham M and Geraci A A 2015 Attonewton force detection using microspheres in a dual-beam optical trap in high vacuum *Phys. Rev.* A **91** 051805
[18] Rodenburg B, Neukirch L P, Vamivakas A N and Bhattacharya M 2016 Quantum model of cooling and force sensing with an optically trapped nanoparticle *Optica* **3** 318
[19] Ranjit G, Cunningham M, Casey K and Geraci A A 2016 Zeptonewton force sensing with nanospheres in an optical lattice *Phys. Rev.* A **93** 053801
[20] Hebestreit E, Frimmer M, Reimann R and Novotny L 2018 Sensing static forces with free-falling nanoparticles *Phys. Rev. Lett.* **121** 063602
[21] Dholakia K and Čižmár T 2011 Shaping the future of manipulation *Nat. Photon.* **5** 335–42
[22] Romero-Isart O, Pflanzer A C, Juan M L, Quidant R, Kiesel N, Aspelmeyer M and Cirac J I 2011 Optically levitating dielectrics in the quantum regime: theory and protocols *Phys. Rev.* A **83** 013803
[23] Kaltenbaek R, Hechenblaikner G, Kiesel N, Romero-Isart O, Schwab K, Johann U and Aspelmeyer M 2012 Macroscopic quantum resonators (MAQRO) *Exp. Astron.* **34** 123–64
[24] Yin Z-Q, Geraci A A and Li T 2013 Optomechanics of levitated dielectric particles *Int. J. Mod. Phys.* B **27** 1330018
[25] Millen J, Monteiro T S, Pettit R and Vamivakas A N 2020 Optomechanics with levitated particles *Rep. Prog. Phys.* **83** 026401
[26] Romero-Isart O, Juan M L, Quidant R and Cirac J I 2010 Toward quantum superposition of living organisms *New J. Phys.* **12** 033015
[27] Chang D E, Regal C A, Papp S B, Wilson D J, Ye J, Painter O, Kimble H J and Zoller P 2010 Cavity opto-mechanics using an optically levitated nanosphere *Proc. Natl Acad. Sci.* **107** 1005–10
[28] Barker P F and Shneider M N 2010 Cavity cooling of an optically trapped nanoparticle *Phys. Rev.* A **81** 023826
[29] Hechenblaikner G, Gangl M, Horak P and Ritsch H 1998 Cooling an atom in a weakly driven high-Q cavity *Phys. Rev.* A **58** 3030–42
[30] Vuletić V and Chu S 2000 Laser cooling of atoms, ions, or molecules by coherent scattering *Phys. Rev. Lett.* **84** 3787–90
[31] Kiesel N, Blaser F, Delic U, Grass D, Kaltenbaek R and Aspelmeyer 2013 Cavity cooling of an optically levitated submicron particle *Proc. Natl Acad. Sci.* **110** 14180–5
[32] Asenbaum P, Kuhn S, Nimmrichter S, Sezer U and Arndt M 2013 Cavity cooling of free silicon nanoparticles in high vacuum *Nat. Commun.* **4** 2743
[33] Millen J, Fonseca P Z G, Mavrogordatos T, Monteiro T S and Barker P F 2015 Cavity cooling a single charged levitated nanosphere *Phys. Rev. Lett.* **114** 123602
[34] Meyer N, Sommer A R, Mestres P, Gieseler J, Jain V, Novotny L and Quidant R 2019 Resolved-sideband cooling of a levitated nanoparticle in the presence of laser phase noise *Phys. Rev. Lett.* **123** 153601
[35] Kuhn S, Wachter G, Wieser F-F, Millen J, Schneider M, Schalko J, Schmid U, Trupke M and Arndt M 2017 Nanoparticle detection in an open-access silicon microcavity *Appl. Phys. Lett.* **111** 253107
[36] Mestres P, Berthelot J, Aćimović S S and Quidant R 2016 Unraveling the optomechanical nature of plasmonic trapping *Light: Sci. Appl.* **5** e16092
[37] Magrini L, Norte R A, Riedinger R, Marinković I, Grass D, Delić U, Gröblacher S, Hong S and Aspelmeyer M 2018 Near-field coupling of a levitated nanoparticle to a photonic crystal cavity *Optica* **5** 1597
[38] Jain V, Gieseler J, Moritz C, Dellago C, Quidant R and Novotny L 2016 Direct measurement of photon recoil from a levitated nanoparticle *Phys. Rev. Lett.* **116** 243601
[39] Gieseler J, Deutsch B, Quidant R and Novotny L 2012 Subkelvin parametric feedback cooling of a laser-trapped nanoparticle *Phys. Rev. Lett.* **109** 103603
[40] Burnham D R and McGloin D 2006 Holographic optical trapping of aerosol droplets *Opt. Express* **14** 4175
[41] Grass D 2018 Levitated optomechanics in vacuum using hollow core photonic crystal fibers and optical cavities *PhD Thesis* University of Vienna
[42] Nimmrichter S, Hammerer K, Asenbaum P, Ritsch H and Arndt M 2010 Master equation for the motion of a polarizable particle in a multimode cavity *New J. Phys.* **12** 083003
[43] Rider A D, Blakemore C P, Gratta G and Moore D C 2018 Single-beam dielectric-microsphere trapping with optical heterodyne detection *Phys. Rev.* A **97** 013842
[44] Ricci F, Cuairan M T, Conangla G P, Schell A W and Quidant R 2019 Accurate mass measurement of a levitated nanomechanical resonator for precision force-sensing *Nano Lett.* **19** 6711–5
[45] Beresnev S A, Chernyak V G and Fomyagin G A 1990 Motion of a spherical particle in a rarefied gas: II. drag and thermal polarization *J. Fluid Mech.* **219** 405
[46] Safavi-Naeini A H, Alegre T P M, Chan J, Eichenfield M, Winger M, Lin Q, Hill J T, Chang D E and Painter O 2011 Electromagnetically induced transparency and slow light with optomechanics *Nature* **472** 69–73
[47] Weis S, Riviere R, Deleglise S, Gavartin E, Arcizet O, Schliesser A and Kippenberg T J 2010 Optomechanically induced transparency *Science* **330** 1520–3
[48] Fleischhauer M, Imamoglu A and Marangos J P 2005 Electromagnetically induced transparency: optics in coherent media *Rev. Mod. Phys.* **77** 633–73
[49] Delic U 2019 Cavity cooling by coherent scattering of a levitated nanosphere in vacuum *PhD Thesis* University of Vienna
[50] Davis E J, Bentsen G, Homeier L, Li T and Schleier-Smith M H 2019 Photon-mediated spin-exchange dynamics of spin-1 atoms *Phys. Rev. Lett.* **122** 10405
[51] Kawasaki A *et al* 2019 Geometrically asymmetric optical cavity for strong atom-photon coupling *Phys. Rev.* A **99** 013437
[52] Delić U, Reisenbauer M, Grass D, Kiesel N, Vuletić V and Aspelmeyer M 2019 Cavity cooling of a levitated nanosphere by coherent scattering *Phys. Rev. Lett.* **122** 123602
[53] Windey D, Gonzalez-Ballestero C, Maurer P, Novotny L, Romero-Isart O and Reimann R 2019 Cavity-based 3d cooling of a levitated nanoparticle via coherent scattering *Phys. Rev. Lett.* **122** 123601
[54] Hauer B D, Maciejko J and Davis J P 2015 Nonlinear power spectral densities for the harmonic oscillator *Ann. Phys.* **361** 148–83